

# $K^0$ and $\Lambda$ production in Ni+Ni collisions near threshold

M. Merschmeyer,<sup>1</sup> X. Lopez,<sup>2,y</sup> N. Bastid,<sup>3</sup> P. Crochet,<sup>3</sup> N. Hermann,<sup>1</sup> A. Andronic,<sup>2</sup> V. Barret,<sup>3</sup> Z. Basrak,<sup>4</sup> M. L. Benabderrahmane,<sup>1</sup> R. Caplar,<sup>4</sup> E. Cordier,<sup>1</sup> P. Dupieux,<sup>3</sup> M. Dzelalija,<sup>4</sup> Z. Fodor,<sup>5</sup> I. Gasparic,<sup>4</sup> Y. Gishkin,<sup>6</sup> O. N. Hartmann,<sup>2</sup> K. D. Hildenbrand,<sup>2</sup> B. Hong,<sup>7</sup> T. J. Kang,<sup>7</sup> J. Keksmeiti,<sup>5</sup> Y. J. Kim,<sup>7,2</sup> M. Kirejczyk,<sup>8</sup> M. Kis,<sup>2,4</sup> T. Matusiewicz,<sup>8</sup> P. Koczon,<sup>2</sup> M. Korolija,<sup>4</sup> R. Kotte,<sup>9</sup> A. Lebedev,<sup>6</sup> Y. Leifels,<sup>2</sup> A. M. Mangiarotti,<sup>1</sup> D. Pelte,<sup>1</sup> M. Petrovici,<sup>10</sup> F. Ramati,<sup>11</sup> W. Reisdorf,<sup>2</sup> M. S. Ryu,<sup>7</sup> A. Schuttauf,<sup>2</sup> Z. Seres,<sup>5</sup> B. Sikora,<sup>8</sup> K. S. Sim,<sup>7</sup> V. Simon,<sup>10</sup> K. Siwek-Wilczynska,<sup>8</sup> V. Smolyankin,<sup>6</sup> G. Stoicea,<sup>10</sup> Z. Tyminski,<sup>8</sup> K. W. Wniewski,<sup>8</sup> Z. G. Xiao,<sup>1</sup> H. S. Xu,<sup>12</sup> I. Yushmanov,<sup>13</sup> X. Y. Zhang,<sup>12</sup> and A. Zhilin<sup>6</sup>

(FOPI Collaboration)

<sup>1</sup>Physikalisches Institut der Universität Heidelberg, Heidelberg, Germany

<sup>2</sup>Gesellschaft für Schwerionenforschung, Darmstadt, Germany

<sup>3</sup>Laboratoire de Physique Corpusculaire, IN2P3/CNRS, and Université Blaise Pascal, Clermont-Ferrand, France

<sup>4</sup>Ruđer Bosković Institute, Zagreb, Croatia

<sup>5</sup>KFKI Research Institute for Particle and Nuclear Physics, Budapest, Hungary

<sup>6</sup>Institute for Theoretical and Experimental Physics, Moscow, Russia

<sup>7</sup>Korea University, Seoul, Korea

<sup>8</sup>Institute of Experimental Physics, Warsaw University, Warsaw, Poland

<sup>9</sup>Institut für Strahlenphysik, Forschungszentrum Dresden-Rossendorf, Dresden, Germany

<sup>10</sup>Institute for Nuclear Physics and Engineering, Bucharest, Romania

<sup>11</sup>Institut de Recherches Subatomiques and Université Louis Pasteur, Strasbourg, France

<sup>12</sup>Institute of Modern Physics, Chinese Academy of Sciences, Lanzhou, China

<sup>13</sup>Kurchatov Institute, Moscow, Russia

(dated: December 18, 2018)

New results concerning the production of neutral strange particles,  $K^0$  and  $\Lambda$  in Ni+Ni collisions at 1.93A GeV, measured with the FOPI detector at GSI-Darmstadt, are presented. Rapidity density distributions and Boltzmann slope parameter distributions are measured in nearly the full phase space of the reaction. The observables are compared to existing  $K^+$  and proton data. While the  $K^0$  data agree with previously reported  $K^+$  measurements, the  $\Lambda$  distributions show a different behavior relative to that of protons. The strangeness balance and the production yield per participating nucleon as a function of the centrality of the reaction are discussed, for the first time at SIS energies.

PACS numbers: 25.75.-q, 25.75.Dw

## I. INTRODUCTION

Strangeness production and propagation in relativistic heavy-ion collisions are active research topics for experimental and theoretical nuclear physics since they are expected to provide interesting opportunities for studying hot and dense nuclear matter. It allows to address fundamental aspects of nuclear physics such as the nuclear Equation of State [1, 2, 3] and the question whether hadronic properties undergo modifications in such an environment [4, 5, 6]. Moreover, it is also of crucial interest to improve our understanding of the reaction mechanisms governing these collisions [7]. The field of heavy-ion physics is also of great importance for astrophysics, in particular to investigate the characteristics of the core of neutron stars [8].

The SIS energy range 1{2A GeV is best suited to study the in-medium properties of strange particles since they are produced below or close to threshold. The den-

sity of the nuclear system created during the reaction is expected to reach up to three times normal nuclear matter density and its temperature is of about 90 MeV [9, 10]. Theoretical works predict that chiral symmetry can be partially restored under those conditions, leading to changes of hadron properties [4, 11] affecting both, production and propagation. Indications for in-medium modifications of charged kaons have been already observed experimentally with data from FOPI [12, 13] and KaoS [14].

Neutral strange particles such as  $K^0$  and  $\Lambda$  are of great interest because of their associated production and the fact that they are not influenced by the Coulomb interaction. The study of their properties may probe the in-medium potential, which is expected to be weakly repulsive for  $K^+$  ( $K^0$ ) [15] and attractive for  $\Lambda$  [16]. It is worth to point out that such opportunity cannot be offered by studies of hypernuclei [17] which allow to investigate the  $\Lambda$ -nucleon potential at normal nuclear matter density.

Detailed studies of the properties of these neutral strange particles have been performed at AGS energies [18, 19, 20, 21, 22]. In this paper new results on the production of  $K^0$  and  $\Lambda$  in Ni+Ni collisions at 1.93A GeV, near threshold (which is 1.58 GeV for free NN collisions),

Electronic address: merschm@physi.uni-heidelberg.de

<sup>y</sup>Electronic address: X.Lopez@gsi.de

are presented. Differential production yields and inverse slope parameters from close to the full phase space are discussed. In particular the high statistics collected during the experiment allows for the first time to investigate the centrality dependence of the  $K^0$  and  $\Lambda$  production yields at SIS energies.

The paper is structured as follows. Section II consists out of a short description of the apparatus. Section III is devoted to the event characterization, namely centrality and azimuthal orientation of the reaction plane. The reconstruction method is detailed in section IV. Section V addresses the experimental results, yields and effective (Boltzmann) slope parameters of  $K^0$  and  $\Lambda$ , which are also compared to existing data of  $K^+$  and proton. Subsequently the strangeness balance and the centrality dependence of  $K^0$  and  $\Lambda$  production are discussed. Finally, a summary and an outlook are given in section VI.

## II. EXPERIMENT

The experiment was performed at the SIS synchrotron of the GSI in Darmstadt (Germany) by bombarding a  $^{58}_{28}\text{Ni}$  beam of 1.93A GeV on an enriched target ( $> 95\%$ ) of  $^{58}_{28}\text{Ni}$ . The target thickness was about  $360 \text{ mg/cm}^2$  corresponding to an interaction probability of 1.5% and the average beam intensity was  $4 \cdot 5 \cdot 10^8$  ions/s.

The FOPPI setup is an azimuthally symmetric apparatus made of several sub-detectors which provide charge and mass determination over nearly the full  $4\pi$  solid angle. The central part ( $23^\circ < \theta_{\text{lab}} < 113^\circ$ ) is placed in a super-conducting solenoid and comprises a drift chamber (CDC) surrounded by a barrel of plastic scintillators for polar angles between  $32^\circ$  and  $72^\circ$ . The mass of particles measured in the CDC is determined using magnetic rigidity and energy loss. The forward part is composed of a wall of plastic scintillators ( $1^\circ < \theta_{\text{lab}} < 25^\circ$ ) and another drift chamber (Helitron) mounted inside the super-conducting solenoid. The plastic wall is divided in two parts: the inner plastic wall and the outer plastic wall (PLAWA) which cover polar angles  $1^\circ < \theta_{\text{lab}} < 6^\circ$  and  $6^\circ < \theta_{\text{lab}} < 25^\circ$ , respectively. The plastic wall provides charge identification of the reaction products, combining time of flight and specific energy loss informations. For the present analysis, the PLAWA and the CDC were used. More details on the configuration and performances of the different components of the FOPPI apparatus can be found in [23].

During the experiment, more than  $110 \cdot 10^6$  events were recorded under "central" and "medium-central" triggers, corresponding to different thresholds on the multiplicity of charged fragments measured in the PLAWA. Most of the events ( $100 \cdot 10^6$ ) were registered under the "central" trigger which accepts events covering up to about 20% of the total reaction cross section.

In previous experiments [10, 12, 13, 24] the target was located at a different position +40 cm in beam direction which led to a better acceptance around target rapid-

ity. With our present target setup, the whole backward hemisphere is covered.

## III. EVENT CHARACTERIZATION

### A. Centrality Selection

The events are sorted according to their degree of centrality by imposing cut conditions on the total charged particle multiplicity measured in both, PLAWA and CDC (i.e. MUL).

Class	$\sigma_{\text{geom in}}$ (mb)	$\sigma_{\text{geom ax}}$ (mb)	$\sigma_{\text{geo}}$ (mb)	$\langle h_{\text{geo i}} \rangle$ (fm)	$A_{\text{part}}$		
MUL1	0	98	98	1.7	0.4	94	6
MUL2	98	389	291	3.6	0.4	63	6
MUL3	398	679	290	4.7	0.3	43	5
MUL4	679	1005	326	5.5	0.3	32	5
Central	0	350	350	3.1	0.4	71	6

TABLE I: Cross section, mean geometrical impact parameter, and number of participants for Ni + Ni collisions at 1.93A GeV for ve different centrality selections (see text for details).

Four event classes are used for the investigation of the centrality dependence of the  $K^0$  and  $\Lambda$  production yields (Tab. I, labeled "MUL1" to "MUL4"). The characteristics of the central event class used to study the  $K^0$  and  $\Lambda$  differential distributions are provided in the last row of Tab. I (labeled "Central"). The corresponding ranges (from  $\sigma_{\text{geom in}}$  to  $\sigma_{\text{geom ax}}$ ) and the portions of the geometrical cross section of the centrality classes ( $\sigma_{\text{geo}}$ ) are listed. The mean geometrical impact parameter  $\langle h_{\text{geo i}} \rangle$  and its r.m.s. deviations are determined assuming a sharp-cut-off approximation [25]. We calculate the average number of nucleons in the reball ( $A_{\text{part}}$ ) using the geometrical model described in [26].

### B. Reaction Plane

When applying the event-mixing technique for the combinatorial background determination one needs to rotate all events into the reaction plane (see section IV). This plane is estimated on an event-by-event basis according to the standard transverse momentum procedure devised in [27] which allows to construct the event-plane vector

$$\vec{Q} = \sum_i \vec{u}_i \quad (1)$$

The sum runs over all charged particles measured in the PLAWA and the CDC. The unit vector  $\vec{u}_i$  is parallel to the particle transverse momentum (i.e.  $\vec{u}_i = (\cos \phi'_i; \sin \phi'_i)$ ), where  $\phi'_i$  is the particle azimuth,

and  $\omega$  is a weight to improve the resolution, depending on the center-of-mass (c.m.) rapidity  $y_{\text{cm}} = y_{\text{lab}} - 0.5 \ln \frac{E + p_z}{E - p_z}$  (the subscript p refers to the projectile):  $\omega = 1$  for  $y_{\text{cm}} < 0.2$ ,  $\omega = +1$  for  $y_{\text{cm}} > +0.2$  and  $\omega = 0$  otherwise. The azimuth of  $Q$  is an estimate of the azimuth of the reaction plane. Typically, the resolution on the reaction plane determination estimated as in [27] from randomly chosen sub-events, is about 30% for central events ( $b_{\text{geo}} = 350 \text{ mb}$ ,  $b_{\text{geo}} < 4.0 \text{ fm}$ ).

#### IV. PARTICLE RECONSTRUCTION

Long-lived neutral strange particles like the  $K_S^0$  or the  $\Lambda^0$  are identified via their charged decay particles in the CDC.  $K_S^0$  and  $K_L^0$  are produced in equal amounts due to the nature of the weak interaction (neglecting CP violation). Because of its lifetime and decay channels the  $K_L^0$  cannot be measured with the FOPI apparatus, whereas the  $K_S^0$  can be reconstructed from its decay into  $\pi^+$  and  $\pi^-$  (branching ratio = 68.6%). Similarly, the reconstruction of the  $\Lambda^0$  is done from the final state containing  $p$  and  $\pi^-$  (branching ratio = 63.9%). A possible contribution to the observed  $\Lambda^0$  comes from the  $\Sigma^0$  which decays exclusively into a  $p$  and a photon. Since the photon cannot be measured with the FOPI detector, and  $\Sigma^0$  cannot be disentangled and are referred to as  $\Lambda^0$  in the following.

The long lifetimes of the weakly decaying  $K_S^0$  ( $c\tau = 2.68 \text{ cm}$ ) and the  $\Lambda^0$  ( $c\tau = 7.89 \text{ cm}$ ) causes a sizeable fraction of these particles decaying somewhat away from the primary vertex. The precision of the track reconstruction in the CDC is sufficient to resolve these secondary vertices. Therefore the signal-to-background ratio is improved significantly by rejecting particles coming from the primary vertex.

##### A. Reconstruction Method

The search for  $K_S^0$  and  $\Lambda^0$  starts with the selection of possible final state particles. Three cuts for each track in the CDC are applied. The first one rejects particles with transverse momenta lower than  $80 - 100 \text{ MeV}/c$  which are spiraling in the CDC. The particle species is selected using the correlation of the particle mass, which is determined from the measured specific energy loss, and the total momentum. The distance of closest approach between track and primary event vertex in the transverse plane is the third quantity. It is used to enhance the fraction of particles coming from secondary vertices in the data sample.

For a jet-type drift chamber like the CDC it is advantageous to pursue a reconstruction strategy which first focuses on the transverse plane ( $x-y$ ) in order to find intersection points of possible decay particle tracks as illustrated in the upper plot of Fig. 1. Once such a point is found, further cut quantities are determined. The transverse distance to the primary vertex  $r_t$  and the closest

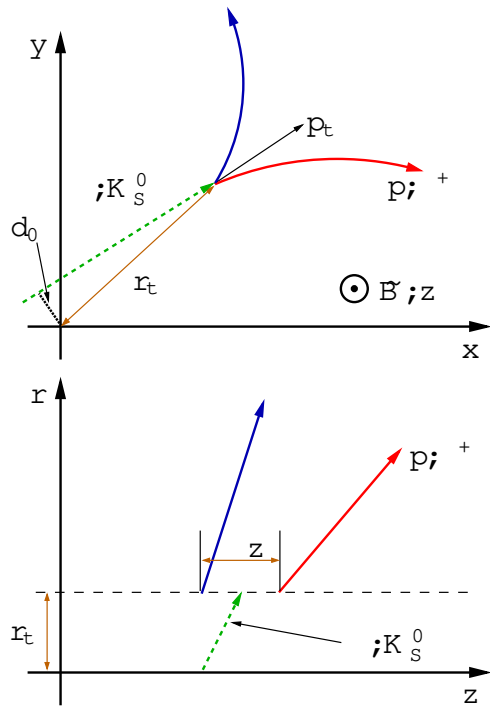


FIG. 1: Schematic view of the  $K_S^0$  and  $\pi^+$  reconstruction in the  $x-y$  plane (top) and in the  $r-z$  plane (bottom). The cut quantities used for the selection of the candidates are illustrated in the plots.

approach of the back-extrapolated mother particle flight path  $d_0$  are used to suppress the background. Then the quality of the signal can be improved by taking into account the longitudinal distance  $z$  of the decay particle tracks as shown in the lower plot of Fig. 1. Afterwards, the invariant mass of the particle pair is calculated from its four-momenta at the intersection point.

##### B. Invariant Mass Spectra and Phase-Space Distributions

The invariant mass spectra of  $\pi^+$  and  $\pi^-$  pairs for a centrality selection of the most central 350 mb of the geometrical cross section are shown in Fig. 2. A total of about  $47 \cdot 10^6$  events were analyzed. The combinatorial background was modeled with the event-mixing method [28]. For that purpose the two decay particle candidates are taken from two different events with the same centrality. In addition, the two events are projected into the same reaction plane. Afterwards, a normalization is applied to the mixed-event background in order to fit the combinatorics in the invariant mass range  $0.56 - 0.80 \text{ GeV}/c^2$  and  $1.15 - 1.25 \text{ GeV}/c^2$  for  $K_S^0$  and  $\Lambda^0$ , respectively. The shape of the resulting mixed-event background fits nicely to that of the combinatorial background and is indicated by the shaded area in Fig. 2. After background subtraction, the remaining peaks in the

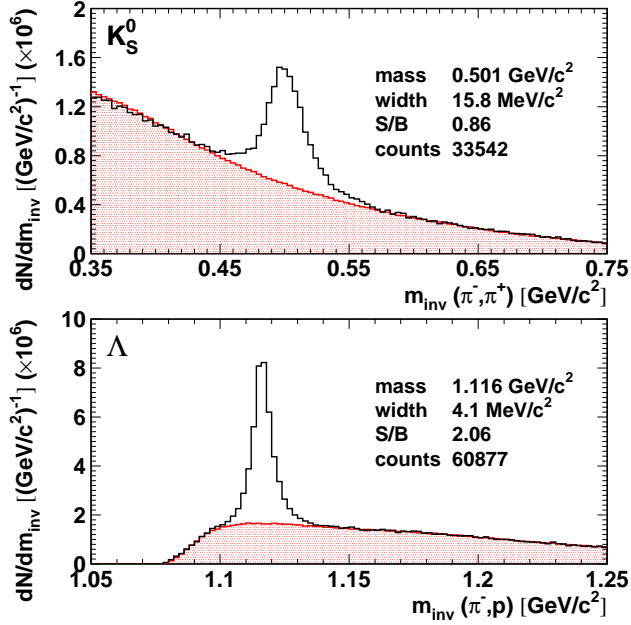


FIG. 2: Invariant mass spectra of  $\pi^+\pi^-$  (top) and  $\pi^-p$  (bottom) pairs. The solid lines denote the combinatorics, the shaded areas represent the scaled mixed-event background.

mass spectra are fitted with Gaussians. Within an interval of  $\pm 2$  around the center of the peak, about 33000  $K_S^0$  and 61000  $\Lambda$  candidates are found for the applied set of cuts in the analysis. The signal-to-background ratios are of 0.9 ( $K_S^0$ ) and 2.1 ( $\Lambda$ ). The (Gaussian) widths of 15.8 MeV/c<sup>2</sup> ( $K_S^0$ ) and 4.1 MeV/c<sup>2</sup> ( $\Lambda$ ) are resulting from the detector resolution.

The background-subtracted phase-space distributions of those particle candidates are presented in Fig. 3 where the transverse momentum  $p_t$  is plotted versus the center-of-mass rapidity  $y_{cm}$ . The solid lines denote the limits of the CDC's polar angular acceptance of 23° and 113° in the forward and backward directions, respectively. Both distributions illustrate the nearly complete coverage of the backward hemisphere. By using the symmetry of the colliding system, most of the phase space becomes accessible. In addition, the  $K_S^0$  distribution shows a fraction of candidates even coming from outside the CDC acceptance. This is possible because both decay particles can still reach the CDC acceptance due to the high excess energy in the decay process.

### C. Acceptance and Efficiency Correction

In order to extract global quantities like the particle yields from the data, the losses due to acceptance and efficiency have to be corrected. For a complex apparatus like the FOPI detector these corrections have to be determined by an extensive GEANT simulation modeling all detector components. The particle distribu-

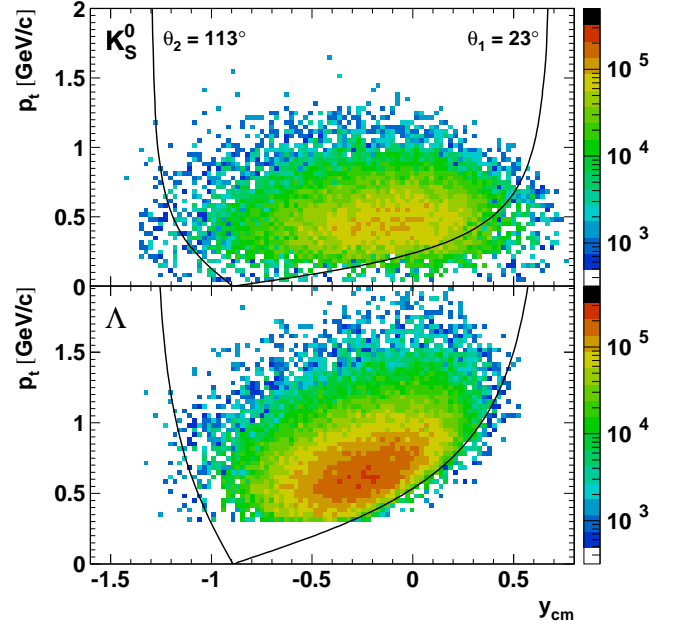


FIG. 3: Phase space distributions of the reconstructed  $K_S^0$  (top) and  $\Lambda$  (bottom), in the plane  $p_t$  vs.  $y_{cm}$ . The solid lines indicate the polar angular coverage of the CDC.

tions of heavy-ion collisions are generated by the IQMD model [9, 29]. The neutral strange particles ( $K_S^0$ ;  $\Lambda$ ) were added separately using a momentum distribution given by the Siemens-Rasmussen formula [30] which describes a system expanding with a temperature  $T$  and a radial expansion velocity  $v_r$ . The choice of the parameters ( $T = 90$  MeV,  $v_r = 0.3$ ) is suggested by previous results obtained for  $\pi$ , protons and deuterons [10].  $K_S^0$  and  $\Lambda$  particles were then embedded into the IQMD output with one  $K_S^0$  and one  $\Lambda$  per event. A full simulation of the detector including resolutions in energy deposition and spatial position, front-end electronics processing and hit tracking, is performed and the resulting output is subject to the same reconstruction procedure as the experimental data. Spectra of all relevant cut quantities were compared between simulated and experimental data [31, 32]. Since no significant differences were found, one can conclude that the detector is properly described by the simulation.

Finally, the reconstruction efficiency is determined by computing the ratio of the number of reconstructed particles in the simulation to the number of particles embedded into the input events. This is done in bins of rapidity  $y_{cm}$  and transverse mass  $m_t m_0$ , where  $m_t = \sqrt{m_0^2 + p_t^2}$  and  $m_0$  is the rest mass of the particle. Thus, the correction method is independent of the choice of the source temperature for the embedded strange particles.

The reconstruction efficiencies for  $K_S^0$  (open circles) and  $\Lambda$  (full squares) are plotted in Fig. 4. The numbers are not corrected for the branching ratio of the respective decay channels. Due to the fact that a minimum trans-

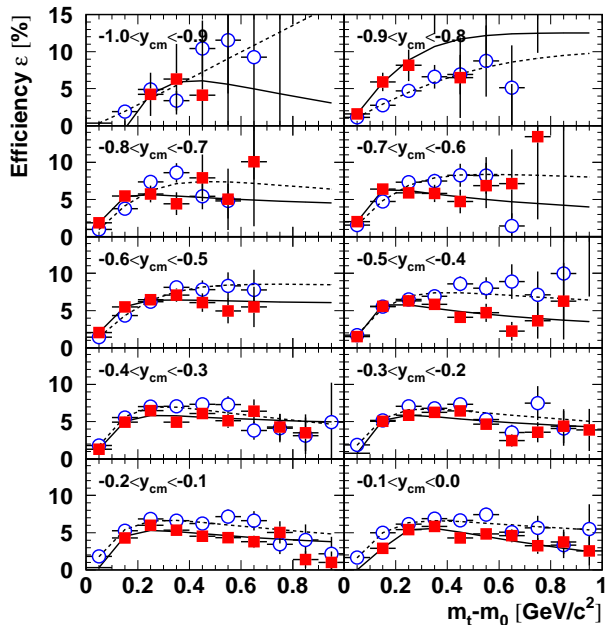


FIG. 4: Reconstruction efficiencies for the  $K_S^0$  (open circles) and the  $\phi$  (full squares) as a function of the transverse mass  $m_t - m_0$  given for different bins of rapidity  $y_{cm}$ . The dashed and solid lines denote fits to the efficiencies of  $K_S^0$  and  $\phi$ , respectively.

verse momentum of 90 (100) MeV/c is requested for the decay particles, the efficiency is low for small values of  $m_t - m_0$  ( $< 100$  MeV/c<sup>2</sup>). At higher transverse masses the efficiencies are approximately independent of  $y_{cm}$  and  $m_t - m_0$  with maximum efficiencies of about 7% for the  $K_S^0$  and 5% for the  $\phi$ , respectively. In order to apply a smooth efficiency correction to the data, which is less sensitive to fluctuations in the high- $m_t$  range, the following function was fitted to the reconstruction efficiencies:

$$f = a \tanh(b(m_t - m_0)) + c(m_t - m_0)^d, \quad (2)$$

where  $a$ ,  $b$  and  $c$  are free fit parameters and  $d$  has a value of 0.45 and 0.2 for  $K_S^0$  and  $\phi$ , respectively. This function was then scaled by the branching ratio of the decay channel and applied to the measured transverse mass spectra.

## V. RESULTS

In this section, the transverse mass spectra of  $K_S^0$  and  $\phi$  after background subtraction and efficiency correction, are fitted with a Boltzmann-type distribution in order to extract the rapidity dependencies of the Boltzmann temperature, the rapidity density distributions and ultimately, the effective temperature and the total production yield in central (350 mb) Ni+Ni reactions at 1.93A GeV. The distributions obtained for  $K_S^0$  and  $\phi$  are

compared to existing data on  $K^+$  and protons, respectively. The large statistics of reconstructed  $K_S^0$  and allows for the first time to discuss the total production yield as a function of the centrality of the reaction, as it has been done at AGS energies [18, 19, 20, 22].

In the following, the results include only statistical errors. Note that the differential yield distribution of the  $K_S^0$  was scaled by a factor two in order to account for the unmeasured contribution from the  $K_L^0$  and is therefore referred to as  $K^0$ .

### A. Transverse Mass Spectra

Figure 5 shows the transverse mass spectra  $m_t - m_0$  of  $K_S^0$  and  $\phi$  particles, after background subtraction and correction for efficiency, branching ratios and the unmeasured  $K_L^0$  contribution, for several rapidity bins indicated in the figure. The rapidity range  $-1.0 < y_{cm} < 0.0$  is covered, hence the full phase space is accessible by exploiting the symmetry of the Ni+Ni system. In order to compile all spectra in one plot they are multiplied by  $10^n$  starting from the lowest spectrum ( $n = 0$ ) to the uppermost spectrum ( $n = 9$ ).

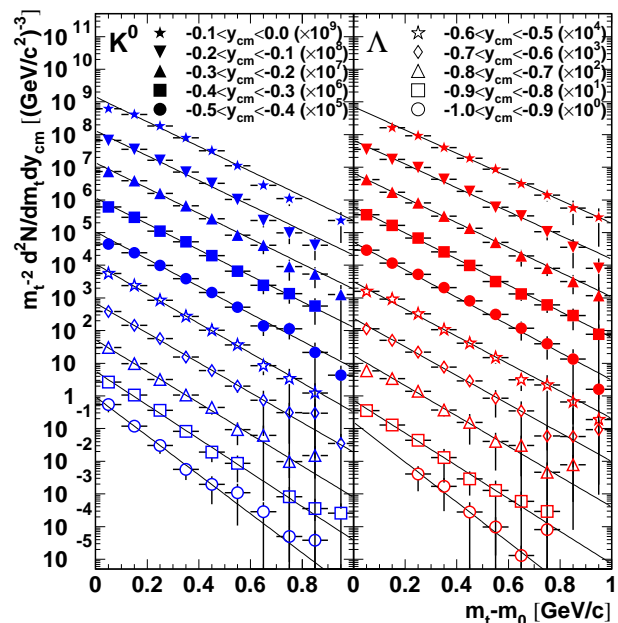


FIG. 5: Transverse mass spectra of reconstructed  $K_S^0$  (left) and  $\phi$  (right). The spectra are plotted for ten rapidity bins ranging from  $y_{cm} = -1.0$  (lowest spectrum, scaled by  $10^0$ ) to  $y_{cm} = 0.0$  (uppermost spectrum, scaled by  $10^9$ ). The data are corrected for the branching ratios of the respective decay channels and the unmeasured  $K_L^0$  contribution.

If particles are emitted from a thermal Boltzmann-like source, their behavior is then described by the following

function:

$$\frac{1}{m_t^2} \frac{d^2N}{d(m_t - m_0)dy_{cm}} = A \exp\left(-\frac{(m_t - m_0)}{T_B}\right) \quad (3)$$

within a narrow window of rapidity  $dy_{cm}$ . Both, the inverse slope parameter ( $T_B$ ) and the integration constant ( $A$ ) depend on the rapidity. This allows to extract the rapidity distributions of the inverse slope parameter  $T_B$  and the rapidity density distributions  $dN=dy_{cm}$  by integrating the fitted function from  $m_t - m_0 = 0$  to 1. In the logarithmic representation, our measured spectra exhibit a linear decrease with increasing  $m_t - m_0$  and are described reasonably well by Eq. 3.

### B. Inverse Slope Parameters

The inverse slope parameter  $T_B$  yields information on the particle temperature at freeze-out for a thermalized system. The Boltzmann temperature  $T_B$  has a simple dependence on the rapidity for an isotropically emitting source:

$$T_B = \frac{T_{eff}}{\cosh(y_{cm})}; \quad (4)$$

where  $T_{eff} = T_B(y_{cm} = 0)$  is the effective temperature, i.e. the slope parameter at mid-rapidity.

The rapidity dependencies of  $T_B$  are depicted in Fig. 6 for various particle species. The full circles and squares indicate measured data points for  $K^0$  and  $\Lambda$  while open symbols denote points reflected with respect to mid-rapidity. The star symbols correspond to previously measured distributions of  $K^+$  [24] and to protons from this experiment. For the  $K^0$  an effective temperature of 114 MeV is extracted from the fit using Eq. 4 which agrees very well with the  $K^+$  results from [42]. The  $T_B$  distribution of  $K^0$  is found to be slightly higher than the one measured for  $K^+$ , within the overlap region. Note that  $K^+$  were measured directly, i.e. via time-of-flight and momentum, and that in previous FOPI experiments the target was in its nominal position which explains the different rapidity range for  $K^+$ . Comparing the combined KaoS and FOPI results for the  $K^+$  to the  $K^0$  suggests that they have very similar freeze-out conditions.

The lower part of the Fig. 6 displays the corresponding results for the  $\Lambda$  with an effective temperature of 119 MeV. They have a somewhat lower freeze-out temperature ( $T_B \approx 20$  MeV) at mid-rapidity as compared to protons. This difference in  $T_B$  is present throughout most of the phase space, only around target and projectile rapidities both measurements agree within errors.

### C. Production Yields

The rapidity density distribution  $dN=dy_{cm}$  is determined separately for each bin in rapidity by an analytic

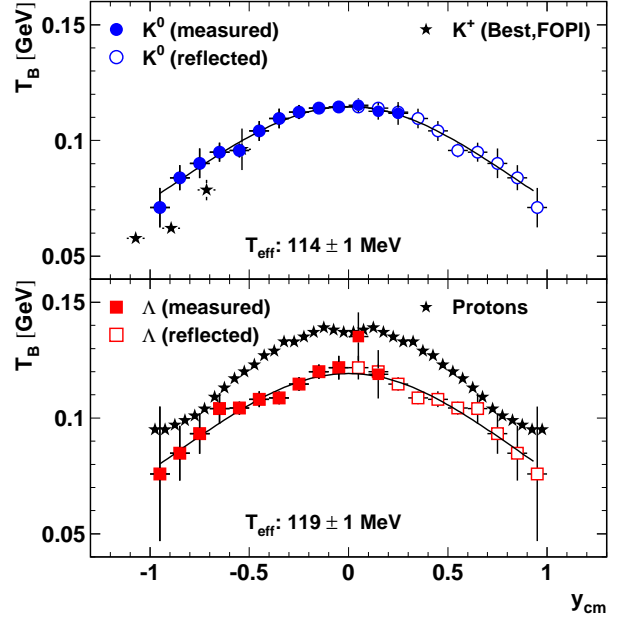


FIG. 6: Rapidity dependency of the inverse slope parameter for  $K^0$  (full circles, upper plot) and  $\Lambda$  (full squares, lower plot). The open symbols are data points reflected with respect to mid-rapidity. The star symbols in the upper plot denote previously measured  $K^+$  [24] and the star symbols in the lower plot denote protons from our experiment. The lines represent a fit assuming an isotropic thermalized source (see text for details).

integration of Eq. 3 from  $m_t = m_0$  to  $m_t = 1$ , using  $A$  and  $T_B$  parameters from the fit. One obtains [33]:

$$\frac{dN}{dy_{cm}} = A \cdot T_B^3 \left( \frac{m_0^2}{T_B^2} + 2 \frac{m_0}{T_B} + 2 \right); \quad (5)$$

where  $m_0$  is the particle's rest mass. Using this method, contributions to the integral from outside the acceptance are included.

The resulting  $dN=dy_{cm}$  distributions are presented in Fig. 7. The meaning of the different symbols is the same as in Fig. 6. The distributions for  $K^0$  and  $\Lambda$  particles are corrected for the corresponding branching ratios. The upper plot shows a comparison between  $K^0$  and  $K^+$  distributions [24, 34], which are found to be very similar. The total  $K^0$  production yield per central (350 mb) collision of 0.078 ± 0.003 and the corresponding width of the  $dN=dy_{cm}$  distribution of 0.493 ± 0.016 are obtained from a Gaussian fit to the data. The combined  $K^+$  distribution has a width of 0.433 ± 0.011 and a total production yield of 0.075 ± 0.002.

The  $dN=dy_{cm}$  distribution of  $\Lambda$  particles is displayed in the lower panel of Fig. 7 and is compared to the one of protons (down-scaled in order to have the same integral as the  $\Lambda$  data). One observes a pronounced longitudinal spread of the proton distribution which could be an indication for a large degree of transparency in the

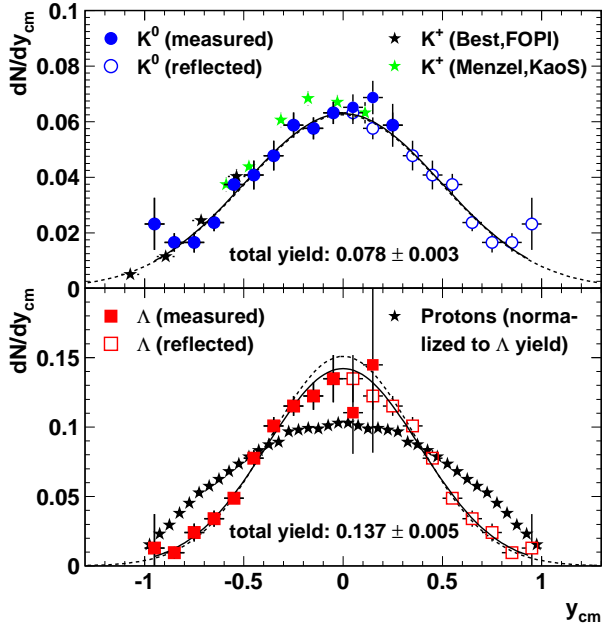


FIG. 7: Rapidity density distributions for  $K^0$  (full circles, upper plot) and  $\Lambda$  (full squares, lower plot). The open symbols are data points reflected with respect to mid-rapidity. The (black and green) star symbols correspond to previously measured  $K^+$  [24, 34] (upper plot) and to protons from this experiment (lower plot). The lines represent a Gaussian fit from which the total production yield is extracted (see text for details).

$Ni + Ni$  system, which has already been found for other systems [35, 36]. The rapidity distribution is much more compact as expected for particles produced in the reball. Such trend is also observed at AGS energies [21]. The total production yield per central (350 mb) collision is  $0.137 \pm 0.005$  and the width of the distribution is  $0.386 \pm 0.009$ .

The dashed curves in both plots denote a Siemens-Rasmussen distribution [30] (normalized to the respective total yield) for a temperature of  $T = 90$  MeV and radial expansion velocity  $\beta = 0.3$  as found in [10]. While the kaons fully agree with the Siemens-Rasmussen distribution, a slight difference is visible for the  $\Lambda$  in the mid-rapidity region. This may indicate a non-isotropic emission of the  $\Lambda$  in the center-of-mass system.

#### D. Evaluation of the Systematic Errors

In order to estimate the systematic error on the width of the rapidity density distributions, on the effective temperatures and on total production yields we apply different sets of cuts by varying the selection criteria of the relevant quantities discussed in section IV. These selection criteria are determined so that it is possible to accept variations of counts in the invariant mass spectra

of about 50%. While the effective temperatures vary within 6(8%) for both particles, the widths of the rapidity density distributions differ by about 6% ( $K^0$ ) and 12% ( $\Lambda$ ). The total production yields change by about 10% ( $K^0$ ) and 18% ( $\Lambda$ ). The systematic errors are summarized in Tab. II.

systematic error of	$K^0$	
slopes [MeV]	+4	+9
dN = dy width	-0.031	-0.031
total yield	+0.007	+0.009
	-0.008	-0.025

TABLE II: Systematic errors on the  $K^0$  and  $\Lambda$  results.

Furthermore, an independent analysis based on a multi-layered neural network [37], also has been used to identify  $\Lambda$  [32, 38]. Within errors the results of yields and inverse slope parameters show a good agreement with the ones obtained from the standard procedure.

#### E. Strangeness Balance

In heavy-ion collisions, strange particles are produced via the strong interaction which conserves the total amount of strangeness in the system. At beam energies of about 2A GeV the bulk part of the produced strange particles comprises the  $\Lambda$  and baryons and the kaons ( $K^+$ ;  $K^0$ ;  $\bar{K}^0$ ). Heavier strange resonances or multi-strange particles have ( $N N$ ) production thresholds which lie significantly above this energy and thus are strongly suppressed. Therefore, their contribution to the overall strangeness production is negligible and will not be considered in the following.

Due to the conservation of strangeness, the balanced sum of the production probabilities of the above mentioned particles then has to cancel:

$$0 = P_{\Lambda} + P_{\Sigma} + P_{\Xi} + P_{\Omega} + P_{K^+} + P_{K^0} + P_{\bar{K}^0} - P_{K^+} - P_{K^0}. \quad (6)$$

Here the symbols of the particles denote the respective strangeness production probabilities. As mentioned earlier, the  $\Xi$  can not be disentangled from the  $\Sigma$  due to its decay properties and to the detector itself. Thus one always measures the  $(\Xi + \Sigma)$  yield. In the case of neutral kaons, one measures the decay of  $K_S^0$  into two charged pions. After acceptance and efficiency corrections one obtains the yield of  $(K_S^0 + K_L^0)$  which is equal to  $(K^0 + \bar{K}^0)$ .

Using the known yields of  $K^+$  [24, 34],  $K^0$  [34],  $K^0 + \bar{K}^0$  and  $\Lambda + \Sigma$  in  $Ni + Ni$  collisions at 1.93A GeV beam energy given in Tab. III, one can now determine

particle	yield	stat. error	syst. error
$K^+$ [24, 34]	0.075	0.002	
$K^-$ [34]	0.003	0.001	
$K^0 + \overline{K^0}$	0.078	0.003	+0:007 0:008
$\Lambda + \Lambda^0$	0.137	0.005	+0:009 0:025

TABLE III: Measured production yields of strange particles in central Ni+Ni collisions (350 mb).

the missing part of the bulk strangeness, i.e. the charged strange baryons  $\Lambda^+$  and  $\Sigma^+$ . These baryons always decay to final states including neutral particles and thus cannot be detected with the FOPI setup. In order to estimate the production yield of charged baryons we use the following relation:

$$\Lambda^+ + \Sigma^+ = K^+ + (\overline{K^0} + \overline{K^+}) - (\Lambda^0 + \Sigma^0) - 3 K^- \quad (7)$$

under the assumption that the number of produced  $\overline{K^0}$  is approximately equal to the number of produced  $K^-$ . The result is a yield of  $0.007 \pm 0.008$  (stat.)  $^{+0:032}_{-0:017}$  (syst.) particles per event (cf. section V D for the determination of the systematic errors). Thus there is very little room for the production of charged (and due to isospin symmetry also neutral) baryons.

This result can be understood partially from the fact that due to the mass difference between  $\Lambda^0$  and  $\Sigma^0$  of about 80 MeV, the thresholds for the direct production in NN collisions are different. While about 1.6A GeV beam energy is needed to produce a  $(\Lambda^0; K^+; \Sigma^0)$  pair, the creation of a  $(\Sigma^0; K^+; \Sigma^0)$  pair requires energies higher than 1.8A GeV. At a beam energy of 1.93A GeV the  $\Lambda^0$  therefore is produced at an excess energy (in the center-of-mass system) of about 125 MeV whereas only 50 MeV are available for the baryons. Thus, one already expects a certain suppression of the  $\Lambda^0$  with respect to the  $\Sigma^0$ .

Experimental studies of p-p collisions by the COSY-11 collaboration [39] have shown that at (center-of-mass) excess energies of a few MeV, the direct production of the  $\Lambda^0$  is suppressed by about a factor 30 relative to the  $\Sigma^0$ . In another experiment by COSY-11, the energy dependence of the  $\Lambda^+$  cross section was investigated [40] and was found to be enhanced by about a factor 10 relative to the  $\Sigma^0$  results. Both, the  $\Lambda^0$  suppression and the  $\Lambda^+$  enhancement seem to be a result of strong final state interactions between the outgoing hyperon and the remaining nucleon.

Evaluating the results of COSY-11 for our situation of different excess energies for  $\Lambda^0$  and  $\Sigma^0$  production, we find a suppression factor of about 30 for the  $\Lambda^0$  with respect to the  $\Sigma^0$  and an enhancement factor of three for the  $\Lambda^+$ . While the  $\Lambda^0$  suppression is fully consistent with our results from the strangeness balance, the  $\Lambda^+$  enhancement is clearly incompatible. Transport and statistical model approaches [41] calculate a  $(\Lambda^+ + \Sigma^+) = (\Lambda^0 + \Sigma^0)$  ratio of

the order of 0.35, while a value of 0.05 is found from our data. A possible explanation could be strangeness exchange occurring in collisions between  $\Lambda^+$  and neutrons with a  $\Lambda^0$  in the final state. This channel would then increase the  $\Lambda^0$  yield and produce the observed behavior of the strangeness balance.

## F. Centrality Dependence

The yield per event of  $K^0$  (full circles) and  $\Lambda$  (full squares) as a function of the centrality (i.e. impact parameter  $b$ , cf. Tab. I) of the reaction is presented in Fig. 8. As expected, the yield per event increases strongly with increasing centrality, for both particles (top panel). One observes an almost linear dependence of the  $K^0$  and  $\Lambda$  production yields on the impact parameter. This has been already observed at AGS energies in Ni+Cu reactions at 2A GeV [18]. Despite the qualitative agreement of both measurements for the  $\Lambda$ , our data show an increase of the production yield from the most peripheral to the most central bin which is about 20% higher than that from the EOS experiment.

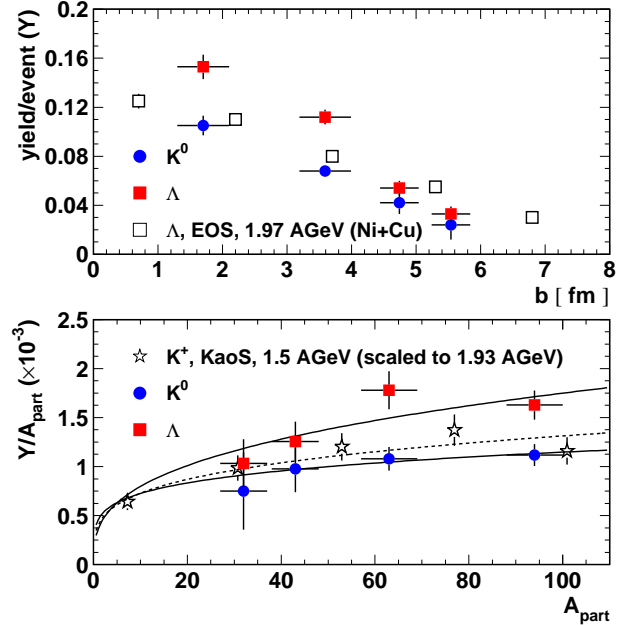


FIG. 8: Upper panel: Yield per event of  $\Lambda$  (full squares) and  $K^0$  (full circles) as a function of the impact parameter  $b$ . The open squares indicate data from the EOS experiment [18]. Lower panel: Yield per event of  $\Lambda$  and  $K^0$  per participating nucleon as function of  $A_{part}$ . The open stars denote experimental results for  $K^+$  from the KaoS experiment [42].

The total yield per event and per participating nucleon ( $P=A_{part}$ ) is plotted as a function of  $A_{part}$  (cf. Tab. I) in the bottom panel of Fig. 8. For both,  $K^0$  and  $\Lambda$ , the yield exhibits a similar rise with  $A_{part}$ , which is of the order of 50% from the most peripheral (MUL4) to the most

central (M U L1) bin. The dependence of  $P = A_{\text{part}}$  on the number of participants can be parameterized by

$$\frac{P}{A_{\text{part}}} / (A_{\text{part}})^{(\kappa - 1)} \quad (8)$$

with  $\kappa = 1.20 \pm 0.25$  and  $\kappa = 1.34 \pm 0.16$  for  $K^0$  and  $\Lambda$ , respectively.

Within errors the  $K^0$  data agree with results on the centrality dependence of the  $K^+$  production yields measured by the KaoS collaboration for the same system [42] (star symbols). Note that for comparison, the KaoS data measured at 1.5A GeV have been scaled by a factor of 3.80 since it was shown that the increase of the  $K^+$  production yield with increasing beam energy ( $E_{\text{beam}}$ ) is proportional to  $E_{\text{beam}}^{5.3 \pm 0.2}$  [43]. Similar trends were also evidenced for  $K^+$  and  $K^-$  measured at lower beam energies in Au + Au and Ni + Ni collisions [42, 44].

The variation of the production yield per  $A_{\text{part}}$  as a function of  $A_{\text{part}}$  can be interpreted as a signature of multiple collisions which are dominantly contributing to the production of strange particles near threshold [43, 45]. Moreover, the similar trends evidenced for  $K^0$  ( $K^+$ ) and  $\Lambda$  allow to conclude that these particles are produced according to the same creation mechanism:  $B B \rightarrow B Y K$  and  $B \rightarrow Y K$ , where B stands for a nucleon or a ( $N$ ) resonance and Y for a  $\Lambda$  or a hyperon, in the 1-2A GeV energy range [7].

Systematically higher values of  $\kappa$  are expected when excluding the most central data point from the fit using Eq. 8. For the  $K^0$  one finds  $\kappa = 1.38 \pm 0.54$  and  $\kappa = 1.84 \pm 0.35$  for the  $\Lambda$ , respectively. The difference between these results and the ones from the full fit mentioned above could imply a saturation of the strangeness production in very central collisions. The effects of the multi-step processes could be partially cancelled by the reshuffling of strange particles by absorption in the large volume of the reball.

## VI. CONCLUSIONS

We have reported on new results from the FOPI experiment concerning the production of neutral strange

particles,  $K^0$  and  $\Lambda$ , in Ni + Ni collisions at 1.93A GeV. A large statistics of high quality  $K_S^0$  and  $\Lambda$  candidates, with a signal-to-background ratio of the order of one to two, have been reconstructed. Phase-space distributions have been measured down to low transverse momenta and in the full rapidity range. Differential yield distributions and inverse slope parameter distributions have been found similar for  $K^0$  and  $K^+$ , confirming that their production mechanisms are identical and that there is no measurable effect of the isospin difference between the two particles. The rapidity distributions of protons and  $\Lambda$  exhibit different trends due to an incomplete stopping in the studied system. Regarding the overall strangeness production, the results request a strong suppression of the charged hyperon production which is not seen in transport or thermal model calculations. The mechanism for this has yet to be found. For the first time at SIS energies, the total production yield of  $K^0$  and  $\Lambda$  per participant is studied as a function of the centrality of the reaction. The increase of the yield with rising number of participants, similar for both  $K^0$  and  $\Lambda$ , indicates that multiple collisions contribute to the production of neutral strange particles near threshold.

All observed trends confirm that  $K^0$  ( $K^+$ ) and  $\Lambda$  production mechanisms are strongly correlated. Detailed comparisons to transport models have to be done in order to check the consistency of the data with the hypothesis of modified in-medium properties of strange hadrons.

## Acknowledgments

This work was partly supported by the German Federal Ministry of Education and Research (BMBWF) under grant No. 06HD 154, by the Gesellschaft für Schwerionenforschung (GSI) under grant No. HD-HER, by the Korea Research Foundation grant (KRF-2005-041-C00120), by the European Commission under the 6th Framework Programme under the 'Integrated Infrastructure Initiative on: Strongly Interacting Matter (Hadron Physics)' (Contract no. RII3-CT-2004-506078) and by the agreement between GSI and IN2P3/CEA.

[1] J. Aichelin, C.M. Ko, Phys. Rev. Lett. 55, 2661 (1985).  
 [2] G.Q. Li, C.M. Ko, Phys. Lett. B 349, 405 (1995).  
 [3] C. Stum et al., Phys. Rev. Lett. 86, 39 (2001).  
 [4] C.M. Ko, V. Koch, G. Li, Ann. Rev. Nucl. Part. Sci. 47 505, (1997) and ref. therein.  
 [5] W. Cassing and E. Bratkovskaya, Phys. Rep. 308, 65 (1999).  
 [6] C. Fuchs, Prog. Part. Nucl. Phys. 56, 1 (2006).  
 [7] C. Fuchs, Z. Wang, L. Sehn, A. Faessler, V.S. Uma Maheswari and D.S. Kosov, Phys. Rev. C 56, R606 (1997); C. Hartnack, J. Jaenicke, L. Sehn, H. Stocker

and J. Aichelin, Nucl. Phys. A 580, 643 (1994).  
 [8] F. W eber, J. Phys. G 27, 465 (2001).  
 [9] J. Aichelin, Phys. Rep. 202, 233 (1991).  
 [10] B. Hong et al., Phys. Rev. C 57, 244 (1998).  
 [11] C.M. Ko and G.Q. Li, J. Phys. G 22, 1673 (1996).  
 [12] P. Crochet et al., Phys. Lett. B 486, 6 (2000).  
 [13] K. W isniewski et al., Eur. Phys. J. A 9, 515 (2000).  
 [14] P. Senger, Prog. Part. Nucl. Phys. 53 1, (2004), and ref. therein.  
 [15] G.Q. Li, C.H. Lee, G.E. Brown, Nucl. Phys. A 625, 372 (1997).

- [16] Z.S. Wang, A. Faessler, C. Fuchs, T. Gross-Boeltling, Nucl. Phys. A 645, 177 (1999).
- [17] D.J. Millener, C.B. Dover and A. Gal, Phys. Rev. C 38, 2700 (1988).
- [18] M. Justice et al, Phys. Lett. B 440, 12 (1998).
- [19] P. Chung et al, Phys. Rev. Lett. 85, 940 (2000).
- [20] P. Chung et al, Phys. Rev. Lett. 86, 2533 (2001).
- [21] S. Albergo et al, Phys. Rev. Lett. 88, 062301 (2002).
- [22] P. Chung et al, Phys. Rev. Lett. 91, 202301 (2003).
- [23] A. Gobbi et al, Nucl. Inst. Meth. A 324, 156 (1993); J. Ritzman et al, Nucl. Phys. (Proc. Suppl.) B 44, 708 (1995); A. Andronic et al, Nucl. Phys. A 679, 765 (2001).
- [24] D. Best et al, Nucl. Phys. A 625, 307 (1997).
- [25] C. Cavata et al, Phys. Rev. C 42, 1760 (1990).
- [26] J. Gosset et al, Phys. Rev. C 16, 629 (1977).
- [27] P. Danielewicz and G. Odyniec, Phys. Lett. B 157, 146 (1985).
- [28] E.L. Berger et al, Phys. Rev. D 15, 206 (1977).
- [29] C. Hartnack et al, Eur. Phys. J. A 1, 151 (1998).
- [30] P.J. Siemens and J.O. Rasmussen, Phys. Rev. Lett. 42, 880 (1979).
- [31] M. Merschmeyer, PhD thesis, University of Heidelberg (2004).
- [32] X. Lopez, PhD thesis, University of Clermont-Ferrand (2004).
- [33] E. Schnedermann, J. Sollfrank and U. Heinz, Phys. Rev. C 48, 2462 (1993).
- [34] M. Menzelet al, Phys. Lett. B 495, 26 (2000).
- [35] B. Hong et al, Phys. Rev. C 66, 034901 (2002).
- [36] W. Reisdorf et al, Phys. Rev. Lett. 92, 232301 (2004).
- [37] V. Breton et al, Nucl. Inst. Meth. A 362, 478 (1995).
- [38] X. Lopez et al, GSI Scientific Report 2002, 2003-1, 49 (2003).
- [39] S. Sewerin et al, Phys. Rev. Lett. 83, 682 (1999).
- [40] T. Rożek et al, Phys. Lett. B 643, 251 (2006).
- [41] A. Andronic, *priv. comm.* (2004); C. Hartnack, *priv. comm.* (2004).
- [42] A. Forster, F. Uhlig et al, Phys. Rev. C 75, 024906 (2007).
- [43] R. Barth et al, Phys. Rev. Lett. 78, 4007 (1997).
- [44] A. Forster et al, Phys. Rev. Lett. 91, 152301 (2003).
- [45] D. Miskowicz et al, Phys. Rev. Lett. 72, 3650 (1994).